Time courses of calcium and calcium-bound buffers following calcium influx in a model cell

Martha C. Nowycky and Martin J. Pinter
Department of Anatomy and Neurobiology, Medical College of Pennsylvania, Philadelphia, PA 19129 USA

ABSTRACT Fixed and diffusible calcium (Ca) buffers shape the spatial and temporal distribution of free Ca following Ca entry through voltage-gated ion channels. This modeling study explores intracellular Ca levels achieved near the membrane and in deeper locations following typical Ca currents obtained with patch clamp experiments. Ca ion diffusion sets an upper limit on the maximal average Ca concentration achieved near the membrane. Fixed buffers restrict Ca elevation spatially to the outermost areas of the cell and slow Ca equilibration. Fixed buffer bound with Ca near the membrane can act as Ca source after termination of Ca influx. The relative contribution of fixed versus diffusible buffers to shaping the Ca transient is determined to a large extent by the binding rate of each buffer, with diffusible buffer dominating at equal binding rates. In the presence of fixed buffers, diffusible buffers speed Ca equilibration throughout the cell. The concentration profile of Ca-bound diffusible buffer differs from the concentration profile of free Ca, reflecting theoretical limits on the temporal resolution which can be achieved with commonly used diffusible Ca indicators. A Ca indicator which is fixed to an intracellular component might more accurately report local Ca concentrations.

INTRODUCTION

Calcium (Ca) ions regulate and coordinate a variety of cellular events including electrical activity, secretion, muscle contraction, protein synthesis, and gene expression. These events are mediated through Ca-sensitive receptors located in distinct cellular regions. The Ca sensor for rapid release of small synaptic vesicles, for example, appears to be located in very close proximity to voltage-gated Ca channels (Llinás et al., 1981; Roberts et al., 1990; Adler et al., 1991). In contrast, slower release of large dense core vesicles, and regulation of protein synthesis or gene expression may occur through sensors located at some distance from the plasma membrane (e.g., Verhage et al., 1991).

Because of the spatially distributed nature of these functions, it is important to understand how Ca becomes distributed throughout the cell following entry through membrane channels or release from intracellular stores. A number of modeling studies have addressed these issues. One group of studies has focused on factors that may determine Ca levels in the immediate vicinity of voltage-gated Ca channels, either while the channels are open or within a few ms of closing (Chad and Eckert, 1984; Fogelson and Zucker, 1985; Simon and Llinas, 1985; Parnas et al., 1989; Yamada and Zucker, 1992; reviewed in Augustine et al., 1987). These studies were motivated by the need to explain very rapid Ca-coupled events which respond to Ca levels that may reach hundreds of μM within a few nanometers of the channel mouth. A different set of modeling studies has estimated free Ca distribution in various parts of the cell over longer durations of several seconds (Smith and Zucker, 1980; Connor and Nikolakopoulou, 1982; Stockbridge and Moore, 1984; Sala and Hernandez-Cruz; 1990). The initial motivation for these studies was the need to interpret signals generated by mobile Ca indicator dyes.

Intracellular Ca buffers or chelators, both fixed and diffusible, play vital roles in determining the distribution of free Ca. The various characteristics of available Ca buffers have been used successfully to study the kinetic properties and location of Ca-triggered events (e.g., Marty and Neher, 1985; Adler et al., 1991). Several recent modeling studies have addressed the question of the effect of buffer properties on Ca transients (Connor and Nikolakopoulou, 1982; Neher, 1986; Sala and Hernandez-Cruz, 1990; see also, Irving et al., 1990). In their comprehensive study, Sala and Hernandez-Cruz (1990) calculated the amplitude and shape of Ca transients resulting from voltage-gated Ca entry in frog sympathetic ganglia neurons for a number of different buffer conditions, such as buffer diffusion rates, affinity, and kinetics. We have modeled Ca transients in a smaller cell (chromaffin cell) and focus more specifically on the influence of buffer kinetics and location. Simultaneously, we consider the distributions of Ca-bound buffers following transmembrane Ca pulses, since such buffers are used to monitor Ca in dye studies. Recent technical advances in confocal microscopy enable the tracking of dye signals with very high spatial and temporal resolution in relatively small cells (Hernandez-Cruz et al., 1990). The modeling presented here considers some theoretical limits on the interpretation of Ca indicator experiments. Finally, we also consider the dynamics of fixed, endogenous buffers during times when Ca levels are changing.

METHODS

Diffusion model

The mathematical model used in this study evaluates the concentration of Ca and other species as a function of time and radial distance in a spherical cell following uniform Ca entry across the outer membrane. The partial differential equation describing this is (Crank, 1975):

Address correspondence to Dr. Martha C. Nowycky, Department of Anatomy & Neurobiology, Medical College of Pennsylvania, 3200 Henry Avenue, Philadelphia, PA 19129, USA.

$$\frac{\partial[S]}{\partial t} = D\left(\frac{\partial^2[S]}{\partial r^2} + \frac{2}{r}\frac{\partial[S]}{\partial r}\right) \quad (1)$$

where $[S]$ is the concentration of the diffusible species, r is the radial distance, and D is the diffusion coefficient.

The model is composed of concentric shells of uniform thickness. The simplifying assumption is made that each of these shells represents a well-mixed system within which diffusion can be neglected. The diffusional properties of each shell are considered to exist only at the shell interfaces and are represented as a set of rate constants after shell surface areas, diffusional distance (shell thickness), and diffusion coefficients are taken into account. This approach is analogous to the "lumped parameter" approach commonly used to solve cable equations (see Rall, 1977). The result of these assumptions is that Eq. 1 can be represented as a system of first-order, ordinary differential equations describing the concentrations for each diffusible species involved in each shell. The convention adopted in this study is that the first shell is outermost and that the Nth shell is innermost. For the ith of N shells, the diffusion equation takes the form:

$$\frac{d[S]_i}{dt} = \frac{D_S}{V_i\delta}\left(A_{i-1}([S]_{i-1} - [S]_i) - A_i([S]_i - [S]_{i+1})\right) \quad (2)$$

where $[S]_i$ is the concentration of diffusible species (Ca or a diffusible buffer), D_S is the diffusion coefficient, δ is the shell thickness, and V_i is the shell volume. A_{i-1} and A_i are, respectively, the surface areas of the outer and inner spherical boundaries of the ith shell. The boundary conditions specify that diffusion does not occur across the outermost spherical boundary or out of the innermost sphere. Thus, the left product within the major parentheses of the right-hand term of Eq. 2 is set to zero for the first (outermost) shell while the right product is set to zero for the Nth (innermost) shell.

Buffers. The rate of change of the concentration of free Ca due to reversible binding with a diffusible or fixed buffer in the ith shell is represented by:

$$\left(\frac{d[Ca]_i}{dt}\right)_B = k_-[CaB]_i - k_+[Ca]_i[B]_i \quad (3)$$

where $[Ca]_i$ is the concentration of free Ca, $[B]_i$ is the concentration of the unbound buffer, $[CaB]_i$ is the concentration of bound buffer and k_- and k_+ are, respectively, the reverse and forward rate constants of the binding reaction. The dissociation constant, k_D, is defined as the ratio of the reverse and forward rate constants (k_-/k_+). This study utilized both diffusible and fixed (non-diffusible) Ca buffers.

Leak and extrusion of Ca. Active extrusion of Ca out of the spherical model from the first shell is defined according to Michaelis–Menten kinetics (Sala and Hernandez-Cruz, 1990). The expression for the rate of change of free Ca from the first shell due to this process is:

$$\left(\frac{d[Ca]_1}{dt}\right)_{Ex} = -V_{MAX}A_1[Ca]_1/V_1([Ca]_1 + K_M). \quad (4)$$

As noted by Sala and Hernandez-Cruz (1990), it is necessary to provide an equal and opposite Ca leak to maintain an initial steady-state prior to applying Ca input to the model. This leak is thus constant and defined by Eq. 4 with the exception that the concentration of Ca used equals the initial "intracellular" Ca concentration (0.1 μM, see Table 1). The use of this concentration guarantees that active extrusion and inward leak of Ca cancel for initial conditions.

Calcium fluxes. The rate of change of free Ca due to influx in the first (outermost) shell is defined by:

TABLE 1 Standard values

Ca diffusion coefficient:	2×10^{-6} cm^2/s
Diffusible buffer (B^D):	
Diffusion coefficient	2×10^{-6} cm^2/s
k_+^D	1×10^7 M$^{-1}\cdot$s^{-1}
k_D^D	0.2 μM
Concentration	0.5 mM
Fixed buffer (B^F):	
k_+^F	1.0×10^8 M$^{-1}\cdot$s^{-1}
k_D^F	5 μM
Concentration	0.5 mM
Initial Ca concentration:	0.1 μM
Ca current:	
Amplitude	0.5 nA
Flux	259×10^{-17} M$\cdot$s^{-1}
Duration	50 ms
Ca extrusion:	
V_{max}	2 pmol/cm$^2\cdot$s
k_M	0.83 μM
Cell radius:	7.5 μ
Shell thickness:	0.1 μ
Time increment:	5 μs

$$\left(\frac{d[Ca]_1}{dt}\right)_{In} = I_{Ca}/2FV_1 \quad (5)$$

where I_{Ca} is the inward Ca current, F is Faraday's constant, and V_1 is the volume of the first shell.

Final model. By combining Eqs. 2–5, a set of linear, first-order differential equations is defined for each shell. For one diffusible (B^D) and one fixed (B^F) buffer, this set takes the following form for the first (outermost) shell:

$$\frac{d[Ca]_1}{dt} = \frac{D_{Ca}}{V_1\delta}(-A_1([Ca]_1 - [Ca]_2)) + \left(\frac{d[Ca]_1}{dt}\right)_{B^D} + \left(\frac{d[Ca]_1}{dt}\right)_{B^F} + \left(\frac{d[Ca]_1}{dt}\right)_{In} + \left(\frac{d[Ca]_1}{dt}\right)_{Leak} + \left(\frac{d[Ca]_1}{dt}\right)_{Ex} \quad (6)$$

$$\frac{d[B^D]_1}{dt} = \frac{D_B}{V_1\delta}(-A_1([B^D]_1 - [B^D]_2)) + \left(\frac{d[Ca]_1}{dt}\right)_{B^D} \quad (7)$$

$$\frac{d[CaB^D]_1}{dt} = \frac{D_B}{V_1\delta}(-A_1([CaB^D]_1 - [CaB^D]_2)) - \left(\frac{d[Ca]_1}{dt}\right)_{B^D} \quad (8)$$

$$\frac{d[B^F]_1}{dt} = -\frac{d[CaB^F]_1}{dt} = \left(\frac{d[Ca]_1}{dt}\right)_{B^F}. \quad (9)$$

Note that the terms describing the Ca leak, extrusion and influx processes are present only in the first shell and that diffusion terms are modified as described above for intermediate and the innermost shells.

Eqs. 6–9 were integrated using a first-order Euler algorithm and written in a FORTRAN subroutine that was linked into ASYST. The ASYST program was run on a PC-compatible computer and allowed the user to select various initial conditions and to perform multiple simulations using ranges of individual parameters.

Parameter selection

Ca diffusion coefficient

The diffusion coefficient of Ca ions in water is 6×10^{-6} cm^2/s (Robinson and Stokes, 1955). The diffusion rate in cytoplasm (in the absence of buffers) is thought to be somewhat slower because of tortuosity. We use a value of 2×10^{-6} cm^2/s, which is based on the rate of movement of barium in the cytoplasm of neurons of the marine gastropod, *Archidoris montereyensis* (Connor et al., 1981).

Diffusible buffer

Diffusion coefficient. The most commonly used exogenous Ca buffers and Ca indicators have a MW of approximately 350 to 800 (EGTA: 380, BAPTA: 476.4, fura-2 analogs: 500–800). The diffusion rate of substances of approximately equal MW in muscle is 2×10^{-6} cm^2/s (Kushmerick and Podolsky, 1969), and this is the value that has been used in this study. Similar values were obtained for fura-2 diffusion in chromaffin cells (Pusch and Neher, 1988) and in lamprey axons (Strautman et al., 1990) and for dinitroBAPTA diffusion in the squid giant synapse (Adler et al. 1991). For simplicity, we assume equal diffusion coefficients for Ca-bound and free buffer.

Diffusible buffer

Kinetic properties. We have used a range of forward binding constants and affinity values to span the experimentally determined properties of a number of commonly used Ca buffers and indicator dyes. The slowest forward binding constants are used to mimic EGTA at physiological pH (Smith et al., 1984), while the fastest are close to values reported for BAPTA and the fura-2, fluo-3 families of Ca indicators (6×10^8 M$^{-1} \cdot$s^{-1}; Grynkiewicz et al., 1985; Kao and Tsien, 1988). Most of the commonly used buffers have affinities (K_D) of 100–200 nM (Smith and Miller, 1985; Grynkiewicz et al., 1985), however, Ca dyes and buffers with lower affinities have been used experimentally (Adler et al., 1991; Augustine and Neher, 1992) and this parameter is varied in one experiment.

Endogenous fixed buffer

In cells which are permeabilized or internally perfused during whole-cell patch clamp recording, endogenous diffusible buffers are washed away. Under these conditions, Ca measurements indicate the presence of endogenous, low affinity, fixed Ca buffers (Smith and Zucker, 1980; Ahmed and Connor, 1988; Thayer and Miller, 1990; Thomas et al., 1990; Neher and Augustine, 1992). We use the recent findings of Neher and Augustine (1992) who estimated that the fixed buffer of bovine chromaffin cells had an affinity (k_D^F) of 5 μM if the total concentration was 0.5 mM, or 10 μM if the total concentration was 0.9 mM.

Little is known of the kinetics of the fixed buffer, except that it must be fast enough to compete with Ca indicator dyes on a ms time scale. We test a number of forward rate constants and for standard conditions use a high value, which emphasizes the influence of fixed buffer. The buffer is assumed to have a homogeneous distribution under standard conditions. The consequences of non-homogeneous distribution are considered in one simulation.

Initial Ca concentration

In almost all cells, basal $[Ca]_i$ is estimated to be 0.1 μM (Carafoli, 1987). Cells appear to be capable of maintaining Ca at this level despite addition of exogenous dyes and buffers (Ahmed and Connor, 1988; Thomas et al., 1990; Neher and Augustine, 1992). In this study, all calculations begin with buffers in equilibrium with 0.1 μM Ca.

Cell size and Ca current amplitude

Values were selected to match ongoing whole cell patch clamp recordings of chromaffin cells. In culture, the cells have a diameter of ~15 μm. Neher and Augustine (1992) estimated that about 95% of chromaffin cell volume is available to Ca dyes, and therefore, our calculations are performed for total cell volume without subtraction of space filling organelles. Ca currents of 0.5 nA are typical for whole cell recordings with elevated $[Ca]_o$ (Nowycky, M. C., and M. J. Pinter, unpublished observations). For simplicity, Ca influx is assumed to occur as a square waveform, without channel inactivation.

Ca extrusion

We included a surface membrane pump for Ca removal using parameters reported by Blaustein (1977) for squid axons. While the properties of the pump are critical for the ultimate removal of Ca, they had essentially no influence on Ca transients during the short intervals used in this study (data not shown).

Distribution of Ca ions in the outermost shell

Within the outermost shell of the model, the Ca concentration is assumed to be uniform. This is equivalent to representing [Ca] as a spatially averaged value located at the midpoint of the first shell (500 Angstroms). In chromaffin cells, voltage-gated calcium channels are relatively uniformly distributed with average channel density calculated as 8.85 channels/μ^2 (Neher, 1986). During channel openings, large Ca gradients are predicted to form around channel mouths. However, these large concentration peaks are spatially restricted to the near vicinity (<50 Angstroms) of channel mouths and are estimated to disappear within microseconds following closure because of rapid diffusion (Simon & Llinás, 1985). Single channel recordings indicate that individual channels "flicker" open and closed during a maintained depolarization, with an open time constant of <1 msec and two closed time constants of 1 and 25 msec (Fenwick et al., 1982; measured at −5 mV). Because of these properties, spatial averaging of Ca may occur when concentrations are considered at relatively remote distances from channel mouths. Thus, the assumption of uniform [Ca] in the outermost shell may be a useful approximation in view of the long duration pulses (50 msec) and relatively thick shell widths used in this study. This assumption would not be warranted, however, when considering Ca or buffer transient profiles at locations in the immediate vicinity of open channnels.

RESULTS

The properties of the model cell were selected to mimic a chromaffin cell under voltage clamp (see section on parameter selection in Methods). The cell radius was chosen as 7.5 μm, and Ca and buffer transients are plotted for shells of 0.1 μm thickness located at 0.1, 1.0, 2.5, and 7.5 μm from the surface membrane. "Peak Ca" refers to the highest concentration in the outermost (sub-membrane) shell during the course of a 50 ms Ca pulse. To better grasp the contributions of buffers and diffusional properties to the spatial and temporal distribution of Ca ions, in the first sections we examine $[Ca]_i$ in the absence of all buffers, then with diffusible buffer alone, and with fixed buffer alone. In the second half of the paper, we study Ca transients in the combined presence of diffusible and fixed buffer.

Ca entry and diffusion rates in the absence of Ca buffers

It is useful to consider first the case of Ca entry in the absence of all buffers since this provides limiting conditions against which all buffers operate. In Fig. 1 *A* calculated free $[Ca]_i$ versus time is plotted in 4 shells under standard conditions for a 50 ms, 0.5 nA pulse. (Note that Ca channel inactivation and effects of decreased driving force for Ca ions in the latter part of the pulse are ignored

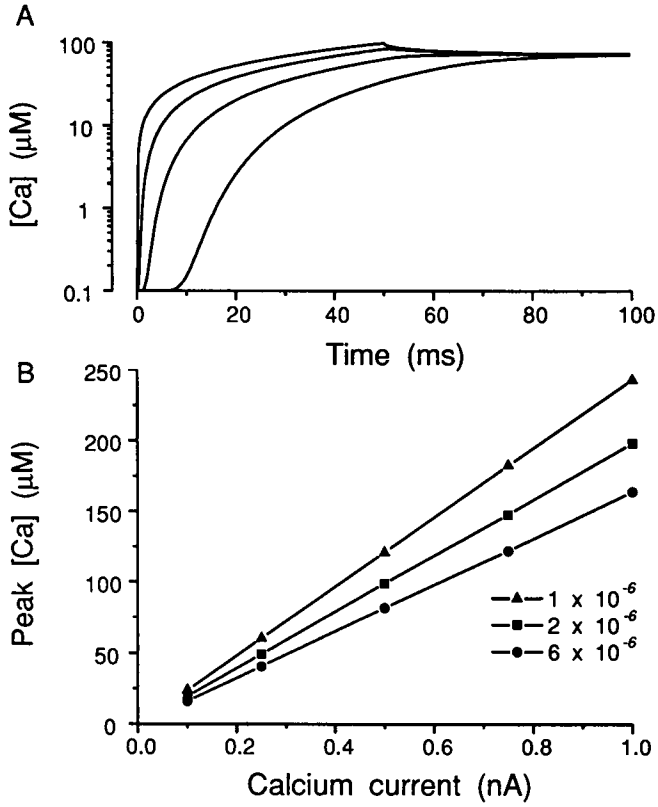

FIGURE 1 In the absence of all Ca buffers, the influx rate and diffusional properties of Ca ions limit maximal $[Ca]_i$ values. (*A*) Ca profiles in 4 shells during the course of a 50 ms pulse and subsequent 50 ms (0.1, 1.0, 2.5, and 7.5 μm from the surface). (*B*) Peak sub-membrane (*shell 1*) Ca achieved during the course of a 50 ms depolarizing pulse for 5 Ca current amplitudes (*influx rates*) and three Ca diffusion rates. Note use of logarithmic scale for [Ca] profiles and linear scale for plot.

in this exercise.) After equilibration (e.g., at 100 ms from pulse initiation), $[Ca]_i$ is 72 μM. Such high levels are never achieved throughout a cell, because they would cause precipitation of hydroxyapatite or other Ca crystals (Kretsinger et al., 1982). However, even under these extreme, non-physiological conditions, peak $[Ca]_i$ levels in the outermost shell are less than 100 μM.

The effects of ion diffusion are quite pronounced in a relatively small cell. For the first ms of the pulse submembrane, Ca increases rapidly (peak rate of 20 μM/ms). For the next few ms, the rates of increase decline, as Ca entry is balanced by radial diffusion, and approach a rate of 1.49 μM/ms. Ca ions reach the innermost shell rapidly, with $[Ca]_i$ beginning to rise in ~10 ms. In the absence of buffers, Ca equilibrates throughout the cell by about 40 ms after pulse termination.

The effect of the rate of Ca influx (Ca current amplitude) and diffusion on peak $[Ca]_i$ in the outermost shell is illustrated in Figure 1 *B*. For 50 ms pulses, peak $[Ca]_i$ values increase almost linearly as a function of Ca current amplitude. The slopes are determined by the Ca diffusion rate and are 240, 200, and 164 μM/nA for diffusion rates of 1, 2, and 6×10^{-6} cm^2/s. The linearity of these plots reflects the absence of buffers and the lack of effect of the Ca pump which possesses slow kinetics. Lower Ca diffusion rates result in slightly higher peak sub-membrane values as Ca accumulates near the point of entry. For the remainder of the study, we will use only the intermediate diffusion rate.

These data emphasize that the rate of Ca influx and diffusional properties have a profound effect on the maximal concentrations that can be achieved in various cellular areas. Exogenous or endogenous Ca buffers can only lower Ca concentrations from these maximum values. Exceptions to this could arise with the presence of physical barriers to Ca diffusion and in the immediate vicinity of open Ca channels.

Diffusible buffer

Effect of forward binding constant

We have simulated the effects of small, organic, diffusible buffers of the type used in whole cell patch clamp experiments. This is of interest for two reasons. First, exogenous buffers such as EGTA and BAPTA are important tools for investigating Ca-mediated events such as secretion, contraction, or the opening or inactivation of ion channels (see Introduction). Second, the most commonly used Ca indicators, e.g., fura-2, are small, mobile Ca buffers with rapid kinetics (Grynkiewicz et al., 1985). Their behavior during Ca transients must be understood to properly interpret the results of Ca measurement experiments. In most of the simulations, we use a two-decade range of forward binding constants which roughly spans experimentally determined values for the relatively slow EGTA to the very fast BAPTA–fura-2 range (see Methods).

In the presence of diffusible buffers, $[Ca]_i$ transients in the outer shells acquire a characteristic "square" or clamped appearance (Fig. 2 *A*1-3). Sub-membrane $[Ca]_i$ rises rapidly to a value which changes only slightly during the remainder of the pulse. This plateau is achieved as Ca influx is balanced by binding to buffer, centripetal diffusion of both free Ca and Ca-bound buffer, and centrifugal diffusion of unbound buffer. At pulse termination, $[Ca]_i$ in the outer shells falls quickly towards equilibrium values.

The forward rate constant of diffusible buffers (k_+^D) powerfully influences several characteristics of the Ca transients. 1) The maximal $[Ca]_i$ levels achieved in the outer shells are strongly dependent on k_+^D. For the 3 k_+^D values tested, peak sub-membrane Ca at the end of a pulse is 18.0, 4.9, and 1.2 μM respectively (Fig. 2 *A*1-3). 2) Faster forward rate constants lowered $[Ca]_i$ more effectively at intermediate cell locations, producing progressively steeper radial gradients of $[Ca]_i$ in the outermost shells during Ca pulses (note 1.0 μm shell in Fig. 2

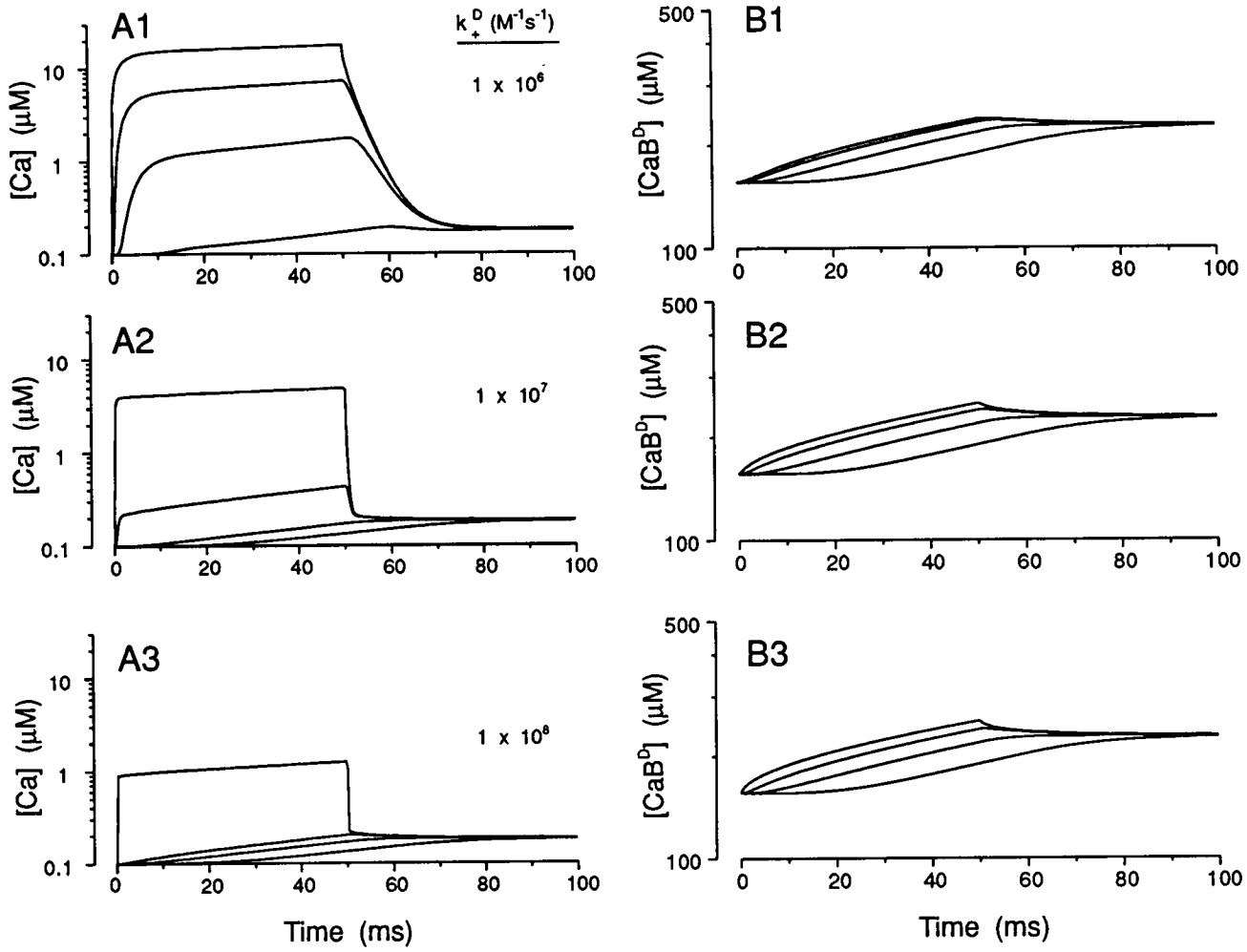

FIGURE 2 Diffusible buffer alone: forward rate constant. (*A*) Ca profiles as in Fig. 1, but with addition of 0.5 mM diffusible buffer. Three sets of 4 traces each, with $k_+^D = 1 \times 10^6$, 1×10^7, and 1×10^8 $M^{-1}s^{-1}$. (*B*) Profiles of bound diffusible buffer for conditions as in *A*. Conditions: Traces are at depths of 0.1, 1.0, 2.5, and 7.5 μm from the surface. Buffer $k_D^D = 0.2$ μM.

*A*1-3). 3) Both the time to reach plateau values and the fall at pulse termination are decreased as the forward rate constant is increased (compare Fig. 2*A*3 to 2*A*1), effects that accentuate the "square" appearance of the Ca transients. (Note that k_D remains constant in these and other simulations in which k_+ is varied.)

The basis for these effects of k_+^D is as follows: As k_+^D is increased, entering Ca is buffered at a higher rate. In the outermost shells, this creates higher local gradients for centripetal flow of bound buffer and centrifugal flow of free buffer (data not shown). Consequently, the flow of free buffer into the outermost shell is increased relative to the influx of Ca, which remains constant in the simulation. These high flow rates of free buffer are maintained for the duration of the influx and are responsible for the rapid drop of Ca in the outermost shell at pulse termination. Thus, diffusible buffers possess a mixing effect that is strongly dependent on the rate of Ca binding. The outcome of this is to speed equilibration throughout the cell, an effect that is barely detectable for a diffusible buffer acting alone, but becomes prominent with the additional presence of fixed buffer (see below).

The concentrations of Ca-bound diffusible buffer are plotted in Fig. 2 *B*1-3 for the three forward binding rate constants. Compared to the effects on Ca transients, variation of the forward rate constant has relatively minor effects on the concentration or spatio-temporal distribution of bound buffer. This arises because, in the presence of adequate supplies of unbound buffer, bound buffer is removed from the outermost shells at higher rates as k_+^D is increased, an effect that serves to maintain bound buffer levels in the outermost shells relatively constant for the three conditions.

Note that the shapes of the Ca-bound buffer transients in the outer shells do not reflect the rapidly changing character of the free Ca transients at pulse initiation and termination. Also, the spatial distribution of free Ca is not represented well by the bound buffer transients.

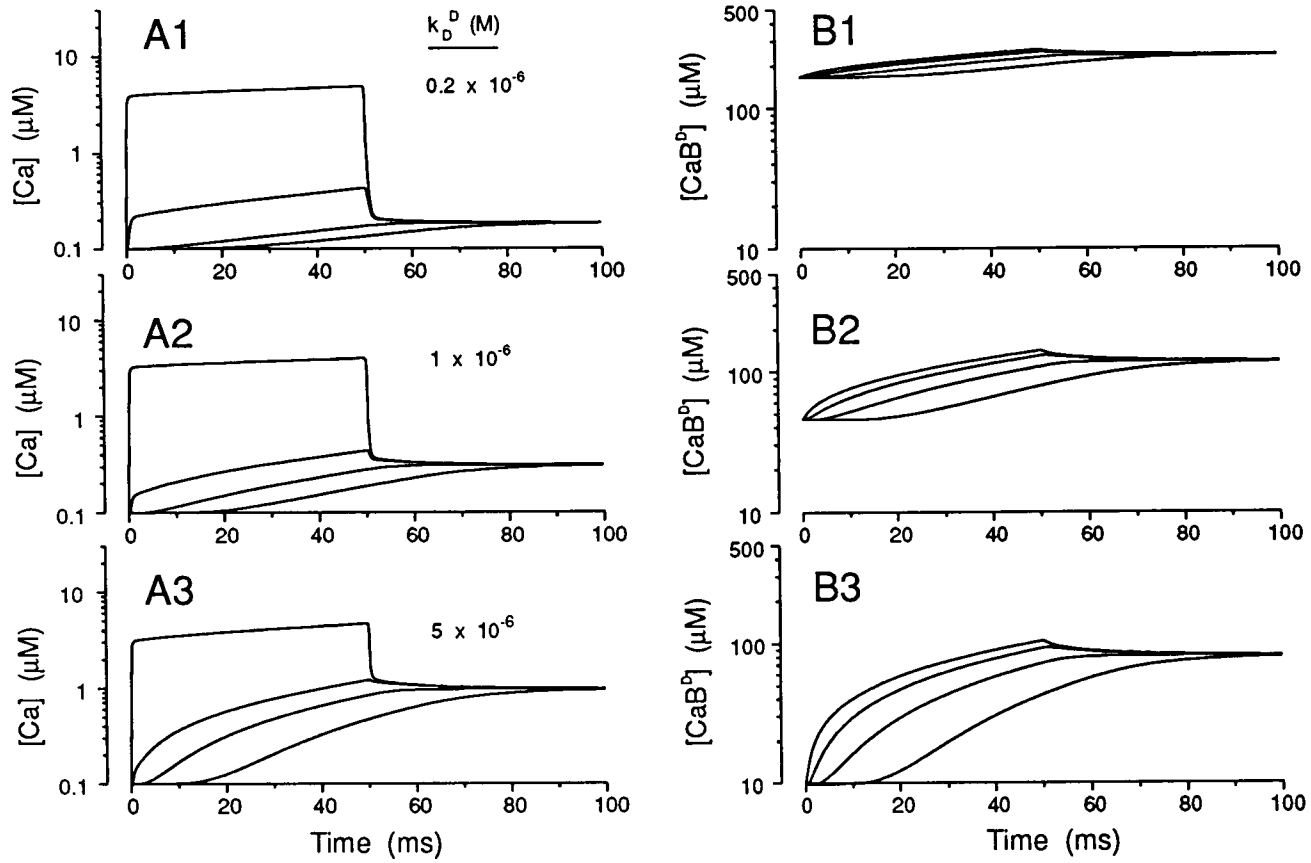

FIGURE 3 Diffusible buffer alone: buffer affinity. (*A*) Ca profiles in the presence of 0.5 mM diffusible buffer. Three sets of 4 traces each, with $k_D^D = 0.2 \times 10^{-6}$, 1×10^{-6}, and 5×10^{-6} M. (*B*) Profiles of bound diffusible buffer for conditions as in *A*. Conditions: Traces are at depths of 0.1, 1.0, 2.5, and 7.5 μm from the surface. Buffer $k_+^D = 1 \times 10^7$ M^{-1} s^{-1}.

These effects are considered further in the context of combinations of fixed and diffusible buffers (see below).

Diffusible buffer

Effect of affinity

The effects of diffusible buffer affinity (k_D^D) on Ca transients were examined for 3 values: 0.2, 1.0, and 5.0 μM (Fig. 3 *A* and *B*). We began with an intermediate k_+^D rate (1×10^7 M^{-1} s^{-1}) and allowed the backward rate constant, k_-^D, to vary.

In these simulations, we set all buffers in equilibrium with 0.1 μM Ca before initiating the pulse. One consequence of varying buffer affinity is a change in the initial amount of available buffer. For the 3 k_D^D values used here, the resulting values of initial available buffer are 333, 455, and 490 μM (Fig. 3 *B*1-3). These amounts are sufficient to adequately buffer the total amount of Ca entering during a standard pulse (72 μM final; see Fig. 1 *A*), and the resulting equilibrium $[Ca]_i$ levels of 0.18, 0.31, and 0.97 μM, respectively (Fig. 3 *A*1-3) are determined primarily by buffer affinity, not availability.

In contrast to equilibrium conditions, the effects of buffer affinity on Ca transients during a pulse are complex. For the 3 k_D^D values, peak sub-membrane Ca levels during a 50 ms pulse are 4.85, 4.01, and 4.69 μM (Fig. 3 *A*1-3). Here, the *highest* affinity buffer paradoxically appears to be *least* effective in buffering peak sub-membrane Ca levels, and the two lower affinity buffers produce values which clearly indicate the existence of further complexities. These results arise from the interactions of several factors. 1) Peak Ca values obtained with the 3 buffers are quite similar because buffer k_+^D is the dominating factor in determining peak Ca during a pulse. In the simulation results of Table 2, the k_D^D is

TABLE 2 Interaction of diffusible buffer affinity and reverse binding constant

k_-^D: k_D^D	2 s^{-1} (k_+^D)	10 s^{-1}	50 s^{-1}
0.2 μM	*(1 × 10⁷)*	*(5 × 10⁷)*	*(2.5 × 10⁸)*
	4.85 μM	1.90 μM	0.72 μM
1 μM	*(2 × 10⁶)*	*(1 × 10⁷)*	*(5 × 10⁷)*
	9.70 μM	4.01 μM	1.65 μM
5 μM	*(4 × 10⁵)*	*(2 × 10⁶)*	*(1 × 10⁷)*
	23.15 μM	10.02 μM	4.69 μM

Calculation of peak free Ca for 3 k_D^D values and 3 k_-^D values. The k_+^D is calculated to give the desired k_D^D value and is printed in small italics above each Ca value.

changed by varying k_+^D with a constant k_-^D, so that the highest affinity buffer also has the highest k_+^D. As k_+^D is decreased, much higher peak sub-membrane Ca are reached (Table 2; compare values within columns). 2) For a given k_+^D, the exact value of peak Ca is determined by the antagonistic interaction of buffer affinity and availability (Fig. 3 *B*). At the start of the pulse there is >100 μM additional available buffer of intermediate rather than highest affinity (Fig. 3 *B*2 versus 3 *B*1). This allows the buffer with the intermediate k_D^D to diminish the Ca transient slightly more effectively than the highest affinity buffer.

The apparently paradoxical effects of buffer affinity on Ca transients are most pronounced in the outermost shell because buffer activity here is dominated by the faster process of Ca binding. In the innermost shells, where changes occur most slowly and therefore approach equilibrium values, there is sufficient time for the lower affinity buffers to release bound Ca, and Ca levels increase proportionately (Fig. 3 *A*2, 3). For the conditions of these simulations, buffer affinity is much less important than the forward rate constant in shaping Ca transients near the membrane, but dominates equilibrium levels, and the extent and rate of Ca increase deeper within the cell.

Fixed buffer

Effect of forward binding constant and affinity

Recent studies with Ca-sensitive dyes suggest that excitable cells possess a large capacity, endogenous, fixed buffer with an affinity that is considerably lower than that of the dyes (see Parameter Selection). We examined the contribution of such a buffer to shaping Ca transients. We also examined the concentration profiles of bound fixed buffer. Since almost nothing is known of the kinetics of the fixed buffer (or, more likely, buffers), we will first explore a two-decade range of forward binding constants (k_+^F), then briefly consider effects of buffer affinity.

Ca transients resulting from a standard pulse in the presence of fixed buffer alone are illustrated in Fig. 4 *A*1-3 using a large total concentration (0.5 mM), low affinity (k_D^F = 5 μM), fixed buffer distributed uniformly throughout the cell. Fixed buffers acting alone dramatically slow Ca equilibration following pulse termination compared with an absence of all buffers (Fig. 1 *A*) or with the action of isolated diffusible buffers (Fig. 2 *A*). In Fig. 4 *A*1, peak Ca levels drop rapidly at pulse termination to a new, but relatively high level which is then maintained for the remainder of the 50 ms shown. This is explained by the fact that at pulse termination, Ca-bound fixed buffers in the outermost shells become local sources of free Ca (Fig. 4 *B*1-3). This Ca-bound buffer generates a Ca gradient which is maintained long after pulse termination because of the large bound buffer capacity and because released Ca ions are liable to be rebound by fixed buffer in neighboring shells.

For the slowest forward rate constant (Fig. 4 *A*1), Ca in the outermost shell rises quickly (<3 ms) to a value which then increases much more slowly during the remainder of the pulse. For longer duration pulses, the secondary slow rise continues approximately linearly until the buffer in the outermost shell approaches saturation (not shown). This qualitative pattern is repeated in deeper shells (shown at 1.0 and 2.5 μm), but with an additional delay due to the time required for unbound Ca ions to diffuse to more central shells. Peak Ca levels in progressively deeper layers are lower, as much of the diffusing Ca is captured by fixed buffer.

As the forward rate constant is increased, fixed buffers slow the rate of rise of $[Ca]_i$ and more effectively limit the spatial extent of $[Ca]_i$ elevation (Fig. 4 *A*2,3). Thus, radial Ca gradients become extremely steep; in Fig. 4 *A*2 and 3 there is almost no Ca increase at 2.5 μm, as more Ca is bound by the fixed buffer in outer shells (Fig. 4 *B*2 and 3). Correspondingly, the Ca profiles rise more slowly in the outermost shells following the pulse onset because of faster binding. $[Ca]_i$ reaches 10 μM in 2.3 ms with $k_+^F = 1 \times 10^6\ M^{-1}\ s^{-1}$, but requires 45 ms with $k_+^F = 1 \times 10^8\ M^{-1}\ s^{-1}$. At higher k_+^F, Ca levels following pulse termination are higher in these locations because of the larger amount of bound buffer acting as a Ca source.

Fig. 4 *B*1-3 illustrate the transients of bound fixed buffer for the identical forward rate constants used in Figs. 4 *A*1-3. Three points regarding these profiles may be noted. First, the bound fixed buffer transients represent the spatial distribution of free Ca to a better extent than do transients of bound diffusible buffer (compare Figs. 2 *B*1-3 with Figs. 4 *B*1-2). Secondly, it may be seen that for the slowest forward rate constants, bound fixed buffer transients do not reflect the rapidly changing temporal features of the associated Ca transients. At the fastest forward rate constant, however, this discrepancy is markedly attenuated as the binding occurs more rapidly and slows the rise of $[Ca]_i$ in the outer shells. Third, the slow increases of bound buffer in the deeper shells particularly following pulse termination are indicators of the slow passage of Ca ions towards the cell center.

We also examined the effect of fixed buffer affinity (k_D^F) using a constant k_+^F (1×10^8) and the same values for k_D^F as in Fig. 3 (0.2, 1.0, and 5.0 μM; data not shown). As for the diffusible buffer, there is little effect on peak Ca levels or profiles in outer shells during a standard pulse, reflecting the dominance of k_+^F in shaping the Ca transient near the membrane. For the higher affinity buffers there is even greater restriction of free Ca and Ca bound buffers to the outer shells. One added complexity created by high affinity fixed buffers was that buffer saturation occurred relatively quickly in the outermost shells, causing sharp increases in the rate of rise of Ca transients.

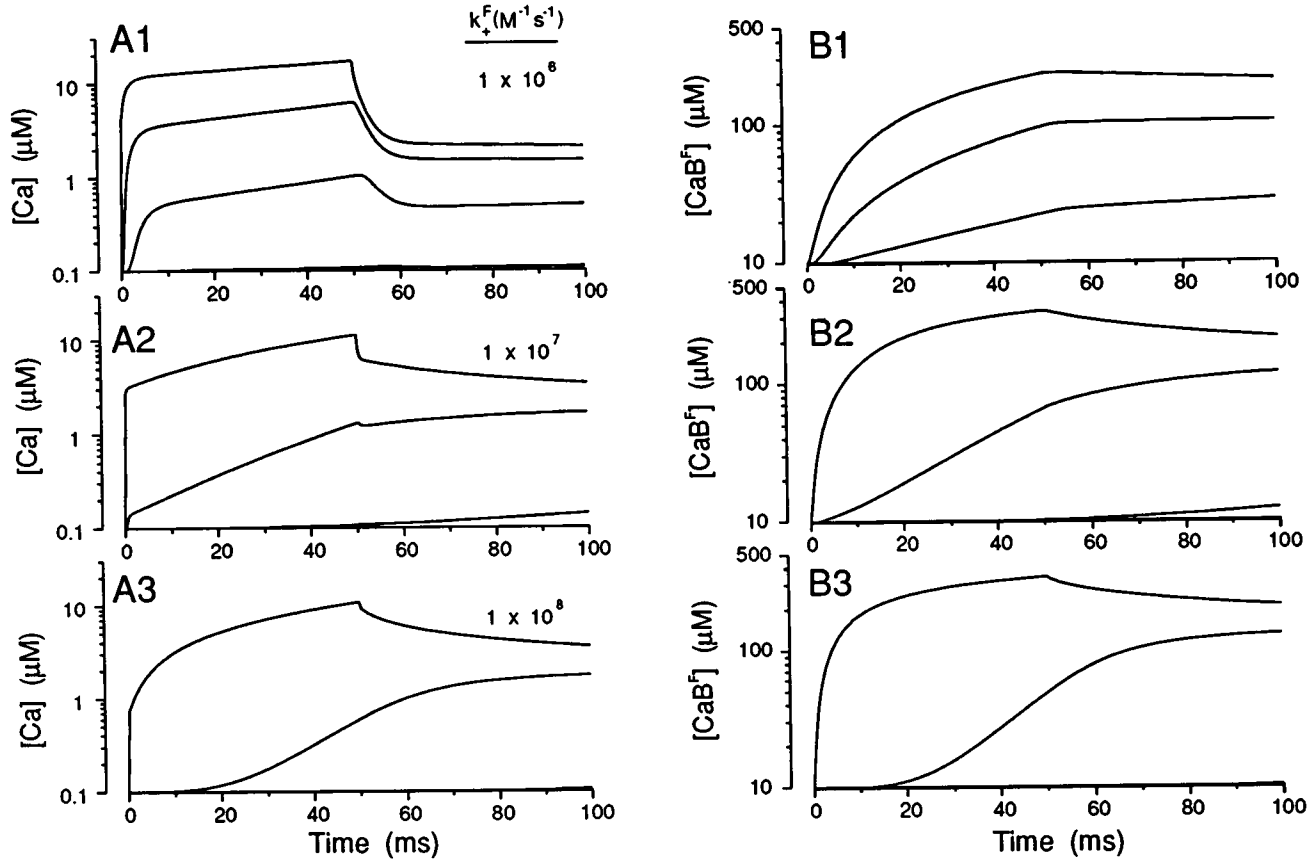

FIGURE 4 Fixed buffer alone: the forward rate constant. (*A*) Ca profiles for the same conditions as Fig. 1, with addition of 0.5 mM fixed buffers. Three sets of 4 traces each, with $k_+^F = 1 \times 10^6$, 1×10^7, and 1×10^8 M^{-1} s^{-1}. (*B*) Profiles of bound fixed buffer for conditions as in *A*. Conditions: Traces are at depths of 0.1, 1.0, 2.5, and 7.5 μm from the surface. Buffer $k_D^F = 5$ μM.

Combination of fixed and diffusible buffers

In this section, interactions between fixed and diffusible buffers are considered. When two such buffers are mixed, the buffer with the higher forward binding constant (k_+) tends to dominate the shape of the Ca transient during the pulse. This is illustrated in Fig. 5 where the k_+ of the fixed buffer is set constant at 1×10^8 M^{-1} s^{-1} and the k_+ of the diffusible buffer is varied at the indicated values. At the slowest k_+^D, the actions of the fixed buffer predominate with most entering Ca bound in the outermost shells, a steep radial Ca gradient present during the pulse and a marked prolongation of Ca equilibration. As the k_+^D is increased, the effects of the diffusible buffer become more apparent; the time to equilibration markedly decreases and the radial Ca gradient during the pulse becomes more compressed. The influence of the diffusible buffer becomes more evident when the two buffers have the same fast forward rate constant (Fig. 5 *A*3); maximal free $[Ca]_i$ is low, the profile in the outermost shell resembles a square pulse of Ca, and equilibration after pulse termination is very rapid. Thus, the mixing effects of the diffusible buffer can compensate for the retarding effect of the fixed buffer on Ca diffusion even when the forward rate constants of the two buffers are equal.

The dominating influence of buffer binding rate during the pulse can also be appreciated by comparing the amounts of bound diffusible and fixed buffers (Fig. 5 *B* and *C*). These are approximately reciprocally related: at the slowest k_+^D (Fig. 5 *B*1), only a small amount of diffusible buffer is bound at the end of the pulse. In contrast, there is a large amount of bound fixed buffer located in the outer shells (Fig. 5 *C*1). This occurs despite the large difference in buffer affinity ($k_D = 0.2$ μM for diffusible, 5 μM for fixed buffer).

Fig. 6 illustrates the effect of increasing the Ca load by increasing pulse duration to 300 ms. All conditions are as in Fig. 5 (3 k_+ rates for the diffusible buffer). For the fastest forward rate constant, the diffusible buffer becomes largely saturated in the later part of the pulse (Fig. 6 *B*3). As this occurs, the Ca levels near the membrane (shell 1) begin to rise steeply (Fig. 6 *A*3) toward a value limited by the action of the fixed buffer and Ca diffusion. The situation is quite different in the presence of the diffusible buffer with the slowest forward rate constant. Ca levels in the outermost shell rise quickly to a value determined largely by fixed buffer binding and Ca diffu-

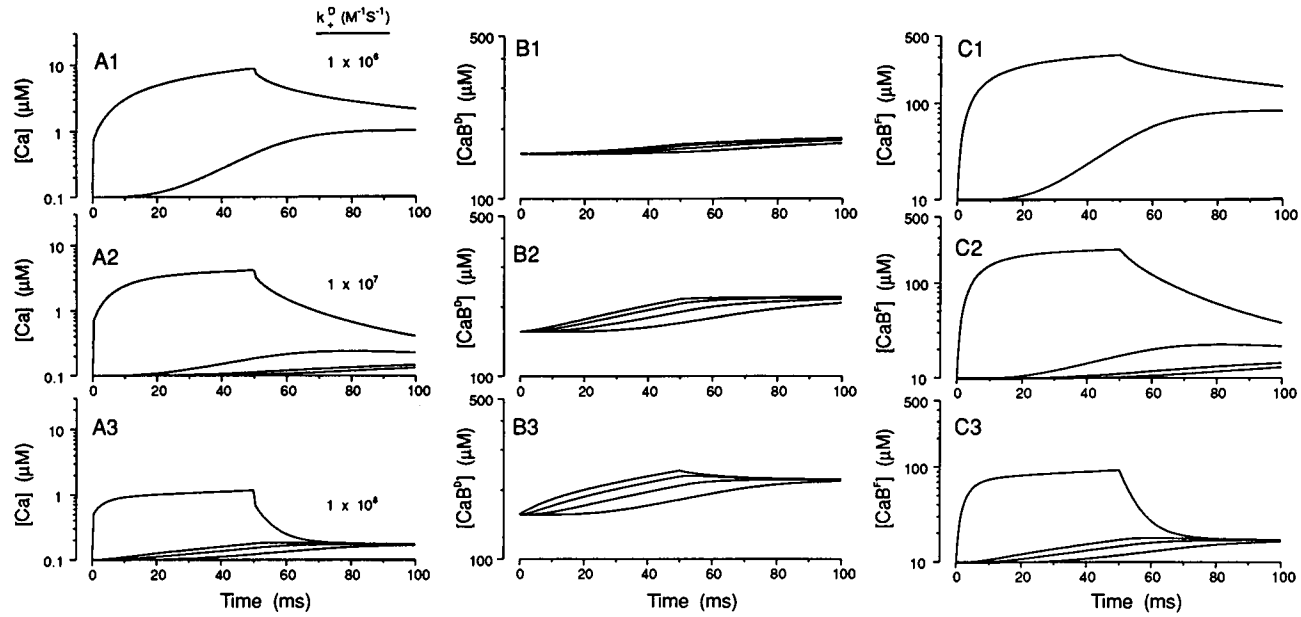

FIGURE 5 Fixed and diffusible buffers combined: forward rate constant of the diffusible buffer. Fixed and diffusible buffers (0.5 mM each) for 1.0 mM total. Three sets of 4 traces each, with $k_+^D = 1 \times 10^6$, 1×10^7, and 1×10^8 $M^{-1} s^{-1}$. $k_+^F = 1 \times 10^8$ $M^{-1} s^{-1}$. (*A*) Ca profiles. (*B*) Profiles of bound diffusible buffer. (*C*) Profiles of bound fixed buffer. Conditions: Traces are at depths of 0.1, 1.0, 2.5, and 7.5 μm from the surface. Diffusible buffer $k_D^D = 0.2$ μM. Fixed buffer $k_D^F = 5$ μM; $k_+^F = 1 \times 10^8$ M^{-1} s^{-1}.

sion, and then increase only slowly during the remainder of the pulse (Fig. 6 *A*1). At the end of the pulse there are still significant amounts of buffer available (Fig. 6 *B*1). Fig. 6 also emphasizes the effectiveness of fast diffusible buffers in distributing free Ca during pulses. With the fastest diffusible buffer (Fig. 6 *A*3), Ca levels in the

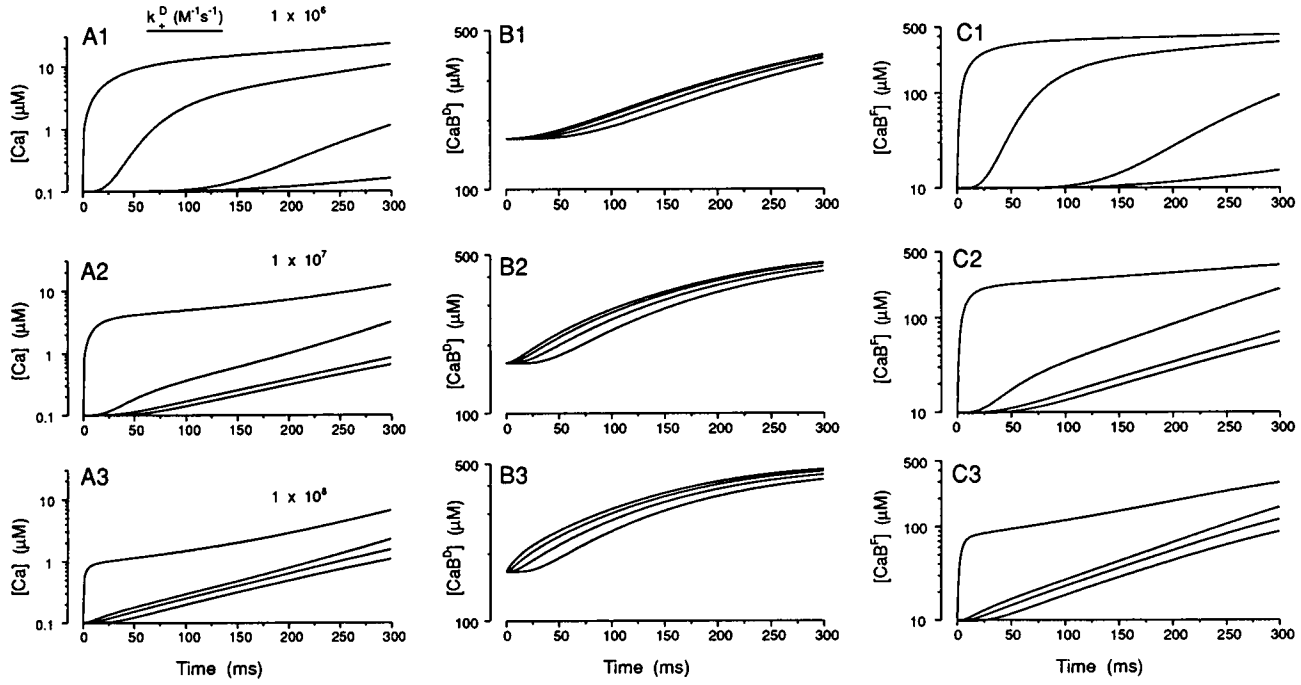

FIGURE 6 Fixed and diffusible buffers combined: effect of prolonged Ca influx. (*A*) Ca profiles in the presence of 0.5 mM fixed and diffusible buffer. Three sets of 4 traces each, with $k_+^D = 1 \times 10^6$, 1×10^7, and 1×10^8 $M^{-1} s^{-1}$. (*B*) Profiles of bound diffusible buffer. (*C*) Profiles of bound fixed buffer. Conditions: Traces are at depths of 0.1, 1.0, 2.5, and 7.5 μm from the surface. Diffusible buffer $k_D^D = 0.2$ μM. Fixed buffer $k_D^F = 5$ μM; $k_+^F = 1 \times 10^8$ M^{-1} s^{-1}.

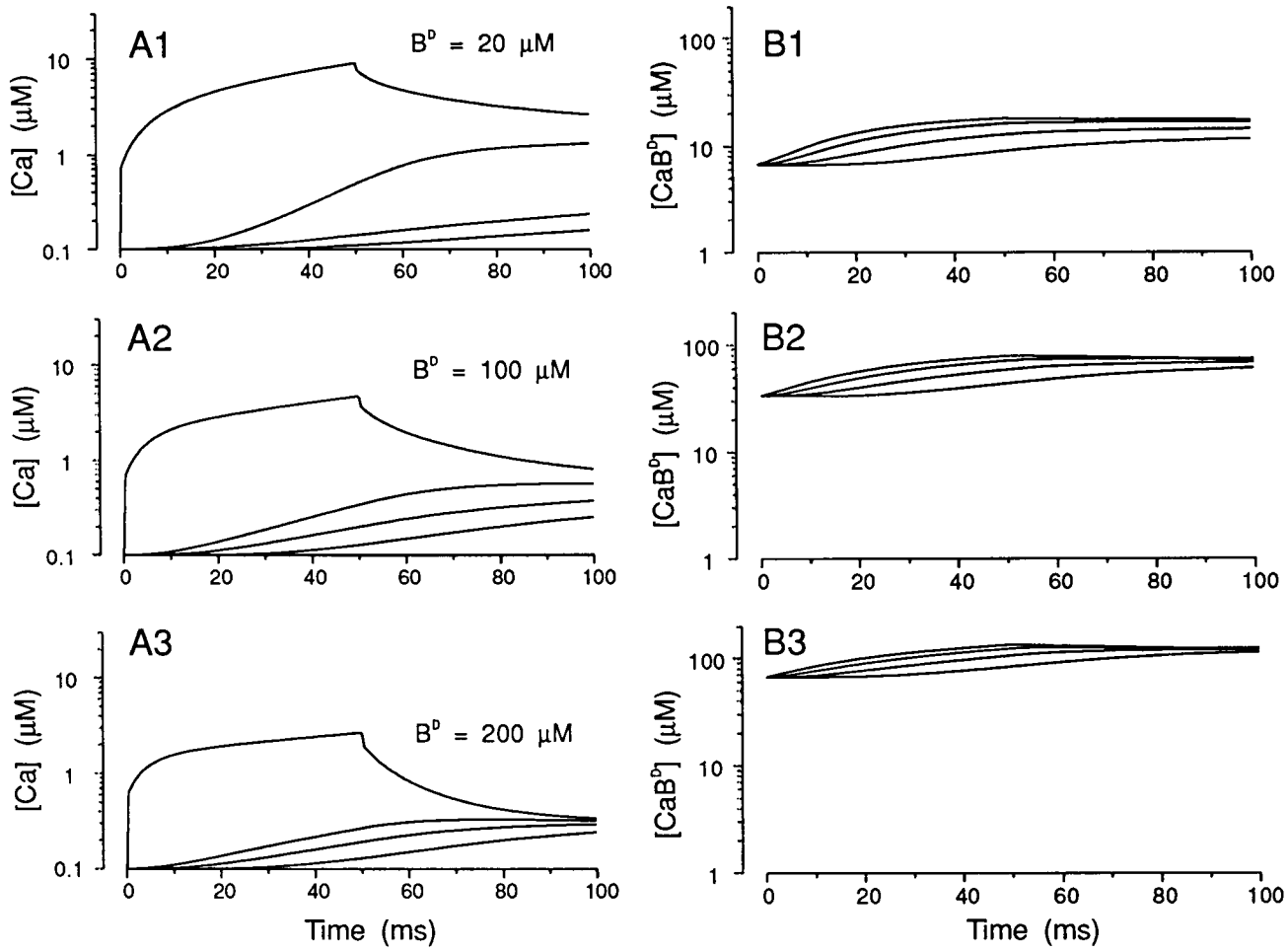

FIGURE 7 Fixed and diffusible buffers combined: effect of low concentrations of diffusible buffer. (*A*) Ca profiles in the presence of 0.5 mM fixed buffer. Three sets of 4 traces each, with concentration of diffusible buffer = 20, 100, and 200 μM. (*B*) Profiles of free diffusible buffer for the same conditions. Conditions: Traces are at depths of 0.1, 1.0, 2.5, and 7.5 μm from the surface. Diffusible buffer $k_D^D = 0.2$ μM; $k_+^D = 1 \times 10^7$ M^{-1} s^{-1}. Fixed buffer $k_D^F = 5$ μM; $k_+^F = 1 \times 10^8$ M^{-1} s^{-1}.

center begin to increase in <50 ms. In the presence of the slowest diffusible buffer (Fig. 6 *A*1), levels in the cell center are barely rising at the end of 300 ms, since most of the Ca is trapped by fixed buffer (Fig. 6 *C*1). In the presence of a low affinity fixed buffer, fast diffusible buffers thus have the effect of restricting the radial gradients of Ca by lowering Ca near the entry points (the membrane) and distributing Ca to deeper cell regions.

In Figs. 5 and 6, it may be seen that the concentration of bound fixed buffer reflects the shape of free Ca transients more accurately than any of the bound diffusible buffers. The shape discrepancy between Ca and bound diffusible buffer transients can also be seen when fixed buffer is not present (Fig. 2). We considered the possibility that decreasing the concentration of diffusible buffer might help to eliminate this discrepancy, but this did not prove to be the case, as illustrated in Fig. 7. This simulation included fixed buffer as in Fig. 5 and a high value of k_+^D for the diffusible buffer. It may first be noted that at the highest concentration (200 μM, Fig. 7, *A*3-*B*3) the profiles of bound diffusible buffer underestimate the extent of Ca radial distribution (also compare to 500 μM buffer in Fig. 5 *A*3). At the lowest concentration (20 μM), saturation of the diffusible buffer in the outermost shells exaggerates this effect. Second, for all shells, the temporal profiles of bound diffusible buffer rise at a slower rate than free Ca and lack the higher frequency components of Ca transients seen in the outermost shells. In general, it appears that transients of bound diffusible buffers are "low-pass" filtered versions of free Ca transients. The effect will thus be most pronounced in cell locations subjected to rapid changes of free Ca. An understanding of this phenomenon should be of importance when evaluating signals obtained using diffusible Ca indicator molecules.

Influence of fixed buffer location

In the preceding simulations, the fixed buffer was distributed uniformly throughout the model cell. In real cells, distribution may be non-homogeneous: an example is

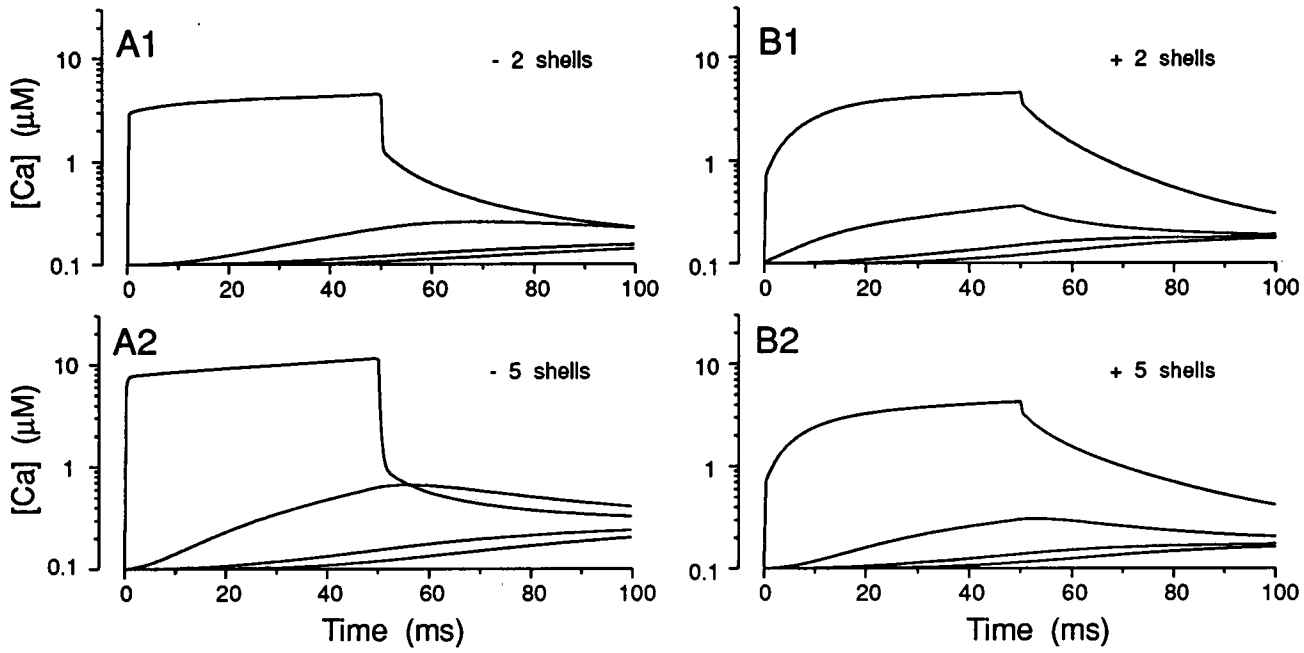

FIGURE 8 Effect of spatial location of the fixed buffer. (*A*) Two sets of 4 traces each, with fixed buffer absent from first 2 shells (0.2 μm) (*A*1), and absent from first 5 shells (0.5 μm) (*A*2). (*B*) Same as *A* but with fixed buffer located only in first 2 (*B*1) or 5 (shells) (*B*2). In both *A* and *B*, 0.5 mM diffusible buffer with standard values was present. Conditions: Traces are at depths of 0.1, 1.0, 2.5, and 7.5 μm from the surface. Diffusible buffer $k_D^D = 0.2$ μM; $k_+^D = 1 \times 10^7$ M^{-1} s^{-1}. Fixed buffer $k_D^F = 5$ μM; $k_+^F = 1 \times 10^8$ M^{-1} s^{-1}.

the spatial localization of smooth endoplasmic reticulum. In Fig. 8 *A*, traces are compared under the conditions of Fig. 5 *A*2, but with the fixed buffer removed from the first 2 (0.2 μm, Fig. 8 *A*1) or 5 (0.5 μm, Fig. 8 *A*2) shells.

Removal of the fixed buffer from even the 2 outermost shells has significant effects on both the peak and rate of rise of sub-membrane $[Ca]_i$. With buffer present in all shells the peak sub-membrane value is 4.18 μM (Fig. 5 *A*1). When the fixed buffer is absent from the first 2 and 5 shells (Fig. 8 *A*), peak values at the end of the pulse in shell 1 are 4.48 and 11.83 μM, respectively. Perhaps more importantly, Ca levels in the first shell reach several μM in a few ms (see below). Fig. 8 *A*2 also demonstrates the importance of fixed bound buffer as a Ca source following the end of a pulse. The Ca levels in shell 10 (1 μm from surface) actually exceed those of the outermost shell after the end of a pulse as bound fixed buffer releases Ca locally.

Fig. 8 *B*1 and 2 illustrate the converse experiment; in these simulations, fixed buffer is confined to the outer 2 (Fig. 8 *B*1) or 5 (Fig. 8 *B*2) shells. It is of interest that the Ca transients in the outermost shell for both conditions do not differ substantially in shape or peak amplitude from the case in which fixed buffer is distributed uniformly throughout the cell (Fig. 5 *A*2). The transient shapes in these location remain distinctly different than when only diffusible buffer is present (Fig. 2 *A*2). It may also be seen that Ca levels in the outermost shells remain considerably elevated following pulse termination. Equilibrium in deeper locations is reached more rapidly, however, reflecting the isolated operation of diffusible buffer in these locations. These simulations demonstrate that the localized operation of a relatively low affinity, but fast, fixed buffer in the immediate vicinity of the membrane can have as much effect on the shaping of sub-membrane Ca transients as when fixed buffer is distributed throughout the cell, even in the presence of a high affinity diffusible buffer.

The changes in the rate of rise of sub-membrane Ca caused by fixed buffers could be significant physiologically. In most excitable cells, Ca enters when voltage-gated Ca channels open during, or just after, an action potential. In many neurons, action potential duration is short, lasting only 1–2 ms, while in most other excitable cells (excluding heart) durations only rarely exceed 10 ms. The location of the fixed buffer will have an important role in shaping the Ca transient.

Peak sub-membrane Ca: effects of diffusible buffer concentration and kinetics and Ca current amplitude

In Fig. 9, the fixed buffer concentration and kinetic properties are kept constant, while both the diffusible buffer concentration and Ca current amplitude are varied. The plots illustrate the peak sub-membrane $[Ca]_i$ achieved during a 50 ms duration pulse for two values of diffusible buffer k_+^D: 1×10^6 (Fig. 9 *A*) and 1×10^8 M^{-1} s^{-1} (Fig. 9 *B*). The data can be considered from two viewpoints: the effect of buffer concentration on a given Ca current am-

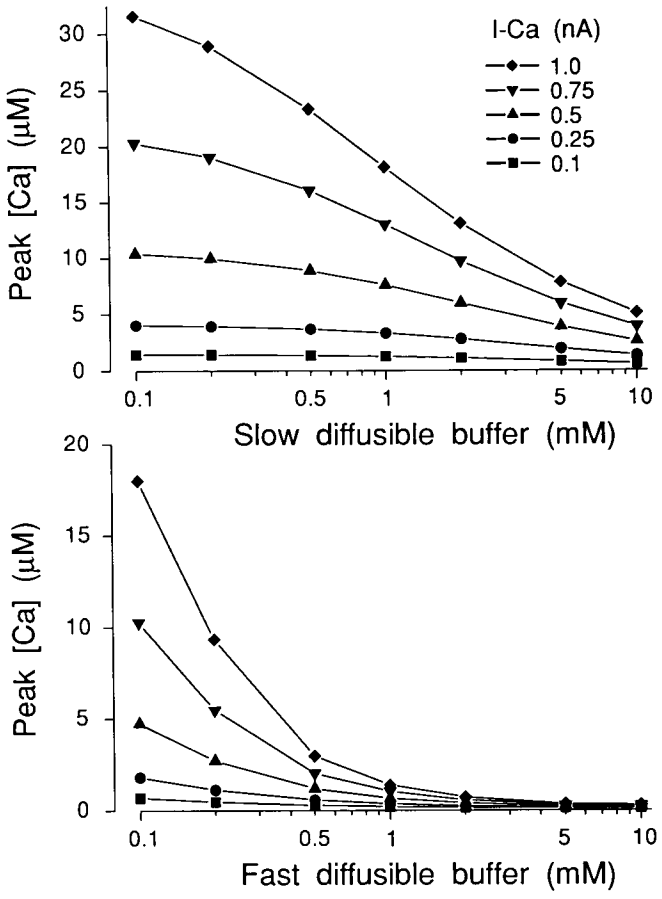

FIGURE 9 Interaction of diffusible buffer concentration, forward rate constant, and Ca current amplitude on peak sub-membrane Ca concentrations. (*A*) Peak values for a 50 ms pulse, standard conditions for 5 Ca current amplitudes. $k_+^D = 1 \times 10^6\ M^{-1}\ s^{-1}$. (*B*) Same as *A*, k_+^D diffusible buffer = $1 \times 10^8\ M^{-1}\ s^{-1}$. Conditions: Diffusible buffer k_D^D = 0.2 μM. Fixed buffer k_D^F = 5 μM; $k_+^F = 1 \times 10^8\ M^{-1}\ s^{-1}$.

plitude and the effect of current amplitudes on a given buffer concentration.

The concentration of a slow diffusible buffer has a surprisingly small effect on peak sub-membrane Ca for a broad range of Ca current amplitude (Fig. 9 *A*). For example, with a 0.5 nA current (*upward triangles*), a 100-fold change in buffer concentration (0.1 to 10 mM) decreases peak Ca from 10.39 to 2.56 μM. At smaller current amplitudes, there is less fractional suppression. At the largest current amplitudes, the difference in peak $[Ca]_i$ for 0.1 versus 10 mM buffer is 31.57 to 5.09 μM (*diamonds*). The results are strikingly different for a fast diffusible buffer (Fig. 9 *B*). Even small concentrations of fast diffusible buffer (e.g., 0.5 mM) reduce peak values significantly, while at higher concentrations (e.g., >1 mM) sub-membrane Ca is well buffered at all current amplitudes.

These results can be understood as follows. If the diffusible buffer is slow, peak sub-membrane Ca is determined largely by the fixed buffer and by Ca diffusion. At lower influx rates a large fraction of Ca binds to the fixed buffer and diffusible buffer has little further effect (see Fig. 5 *B*1). At higher influx rates, Ca increases as Ca entry exceeds both the ability of the fixed buffer to bind and the rate of removal by Ca diffusion. It is only then that the concentration of diffusible slow buffer exerts a noticeable effect. Note that the faster *fixed* buffer dominates the peak Ca transient even though the affinity of the diffusible buffer is very high compared to that of the fixed buffer. In contrast, a fast diffusible buffer competes effectively with the fixed buffer. Ca levels are lowered by the combination of diffusion of free Ca, and by Ca removal in a buffer-bound state. With this combination of forces, Ca currents of different amplitudes are more readily clamped by relatively small amounts of buffer.

The data can also be examined for how effectively a given concentration of diffusible buffer lowers Ca currents of different amplitude near the membrane. It is readily apparent that even high concentrations of a slow diffusible buffer would result in widely different concentrations of peak sub-membrane Ca, depending on current amplitude. Low concentrations of fast diffusible buffer would also be poor Ca clamps for currents of different magnitude.

It is important to note that the effects of buffer concentration illustrated in Fig. 9 are restricted to the outermost shells. Inner shells are subject to other influences (see Fig. 5 *A*1 and 3 to contrast effects on the tenth and central shells in slow and fast buffers). As expected, higher buffer concentrations exert greater effects at equilibrium, and in deeper shells.

DISCUSSION

This study explores several aspects of Ca distribution throughout a spherical model cell following influx across an outer membrane. In their modeling study, Sala and Hernandez-Cruz (1990) focused on several factors which influence Ca transients such as pulse duration, buffer diffusion rates, buffer affinity and kinetics, and Ca extrusion by a membrane pump. Here we extend this analysis, concentrate on brief Ca transients, and perform a more detailed analysis of the effects of both diffusible and fixed buffer kinetics in shaping these transients. We also consider the dynamics of Ca-bound buffers for several reasons: first, knowledge of their behavior aids in understanding how they shape Ca transients, and second, both Ca-measuring dyes and physiological Ca sensors are Ca buffers and their behavior during Ca transients has intrinsic interest. Finally, information on the effects of diffusible buffers with various kinetic properties is useful for manipulating Ca transients experimentally.

Upper limits to free Ca

All buffers, endogenous and exogenous, can only lower Ca levels from upper limits imposed by the balance of Ca

influx and diffusion in the absence of buffers (Fig. 1). Three factors could increase the peak values under such conditions. First, if Ca diffusion were slowed by the presence of physical barriers to ion movement, local "hot spots" of Ca accumulation could exist. Second, larger Ca currents would produce higher sub-membrane Ca levels by shifting the initial balance between influx and diffusion. Third, clustering of channels would produce higher levels in the first few shells before Ca ions diffuse laterally and radially. It is important to recognize the existence of these practical limits for Ca-activated processes that are more than a short distance (e.g., 100 nm) from the mouth of voltage-gated Ca channels. Ca sensors with a Ca affinity in the hundreds of μM do exist: Ca-activated ion channels and the receptor for fast secretion are two examples. However, these very low affinity sensors must be located very near Ca channels (Augustine et al., 1987; Roberts et al., 1990; Adler et al., 1991). Ca sensors farther from the membrane, or in cells without Ca channel clustering, must have much higher affinities. Indeed, many small, endogenous Ca sensors have k_D values of 1 μM or less (Carafoli, 1987).

Exogenous diffusible buffers as experimental tools

Small diffusible buffers with various combinations of buffer affinities and kinetic properties constitute a valuable set of tools to probe Ca-mediated events (e.g., see Marty and Neher, 1985; Adler et al., 1991). Four features of Ca elevation in response to Ca entry can be manipulated by the buffer properties considered in this study: 1) peak Ca levels near the membrane; 2) spatial distribution of elevation; 3) duration of elevation; and 4) post-pulse equilibrium levels.

The forward binding constant of the diffusible buffer is the single most potent kinetic parameter explored in this study for determining the shape and height of Ca transients near the membrane and restricting radial spread of Ca elevation. Buffer affinity has the expected effects on free Ca at post-pulse equilibrium, but little or no effect on peak levels near the membrane, if the forward binding constant is fast. However, even in the presence of a rapid forward rate constant, lower affinities can significantly increase the spatial extent of Ca elevation (compare Fig. 3 *A*1 with 3 *A*3). On the other hand, a buffer with lower affinity with a lower forward binding constant will allow peak Ca transients near the membrane to increase (Table 2). By using different buffer concentrations, many of these effects can be exaggerated. For example, a higher concentration of a slow, EGTA-like buffer can be selected to keep Ca transient amplitude near the membrane approximately equal to that produced by a lower concentration of a fast, BAPTA-like buffer (Fig. 9), but would buffer Ca levels in deeper shells more effectively. Equimolar buffers of different affinities but equal forward rate constants would set post-stimulus Ca to different levels, with little effect on transients near the membrane. Thus, buffers could be used to identify both the Ca requirements and location of Ca sensors for cellular events. Given the limited temporal and spatial resolution of current Ca imaging and detection techniques, it may be more useful to experimentally manipulate Ca levels rather than trying to determine them.

Ca-bound buffers: Ca dyes

The experiments performed in this modeling study provide some insights into theoretical limits on the temporal and spatial resolution of the "Ca signal" which can be obtained with small, high-affinity, diffusible dyes, such as the fura or fluo families (Grynkiewicz et al., 1985; Kao and Tsien, 1988). Several reports have noted that even very low concentrations of mobile Ca dyes distort the shape and amplitude of free Ca transients, an effect related to the buffering action of these dyes (Sala and Hernandez-Cruz, 1990; Neher and Augustine, 1992). However, to our knowledge, no one has noted that the spatio-temporal profiles of the Ca-bound or unbound forms of the dyes do not accurately reflect rapid Ca changes or gradients. Experimentally, the flourescence of a compound such as Fura-2 is measured and converted to Ca concentration using ratiometric calibration equations (Grynkiewicz, et al., 1985). A simulation of this procedure indicates that the Ca concentration may be considerably underestimated in the outermost shells where it is changing rapidly and overestimated to a smaller extent in deeper shells where it changes less rapidly (data not shown).

This observation has important implications for the potential effectiveness of mobile compounds as Ca indicators when the Ca concentration is changing rapidly. Synthesis of higher affinity dyes which can be used at lower concentrations will not improve this situation (indeed, low concentrations simply saturate rapidly). Instead, fixed buffers have more potential for accurately reporting local Ca transients. An ideal "designer" dye might be one which is mobile in saline, but binds to a uniformly distributed cellular constituent and acts as a Ca indicator only in a Ca-bound, fixed state. Of course, such a dye will also distort Ca transients and be susceptible to saturation near sites of Ca entry, but theoretically, the optical measurements should be easier to translate into free Ca levels. Fura-2 actually fulfills some of these criteria in skeletal muscle cells, where its diffusion is retarded by a cellular constituent to much lower values than in saline or the cytoplasm of many cells (Konishi et al., 1988).

Fixed buffer

We incorporated a fixed buffer which has been inferred to exist on the basis of Ca-imaging data (see Parameter Selection). Unfortunately, little is known about the detailed kinetic properties and distribution of fixed endoge-

nous buffers, which may consist of heterogeneous populations of cellular constituents. In the absence of detailed experimental information, we have attempted to indicate some of the effects which would be expected from changes in buffer binding constants, affinities, and distribution. Although we only explored a narrow range of parameters, several qualitative conclusions can be made.

1) The presence of fixed buffers greatly retards Ca diffusion as originally pointed out by Hodgkin and Keynes (1957). Stockbridge and Moore (1984) calculated that in the presence of fixed buffer alone, Ca equilibration in a 1 μm diameter nerve terminal would require many tens of ms. Our study demonstrates the competing interactions of mobile buffer kinetics (particularly forward binding rates) in speeding Ca equilibration in the presence of equimolar concentrations of fast fixed buffer. 2) In the absence of mobile buffers, bound fixed buffer acts as a source of Ca which will prolong the amount of time that Ca is elevated in areas near sites of Ca entry. 3) A non-homogeneously distributed fixed buffer will act to protect local areas from Ca transients, as pointed out by Sala and Hernandez-Cruz (1990). Such a mechanism may be important, for example, in shielding lengths of axons from Ca entry into boutons or restricting Ca entry into individual dendritic spines. 4) Finally, a fixed buffer localized near sites of Ca entry could slow the rate of rise of the Ca transient near the membrane (Fig. 8), which may be important in cells with brief action potentials.

Our study also provides some interesting qualitative information about the dynamics of fixed buffers, which may have physiological significance. Some Ca mediators of cellular events must be fixed (or diffuse extremely slowly), since Ca-dependent events such as exocytosis or ion channel activation or inactivation are observed despite prolonged perfusion by whole cell patch clamp recordings. The results of modeling Ca-bound fixed buffer suggest that knowledge of Ca transients alone may not be sufficient for predicting the degree of bound fixed buffer. Bound fixed buffer is very sensitive to the history of Ca entry, degree of Ca binding, and diffusion. As noted by Yamada and Zucker (1992), a fixed buffer with slow kinetics and located in the outer shells can "remember" Ca entry from one action potential to another and act as a Ca entry integrator (Fig. 4). The "residual Ca" hypothesis of transmitter release may need to be supplemented with a "residual bound fixed buffer" hypothesis.

Conclusion

This modeling study arose from a need to understand the effects of exogenous buffers on Ca-stimulated exocytosis in small, secretory cells maintained under whole-cell patch clamp (Seward et al., 1992). It is interesting to speculate about the applicability of these results to intact cells that are known to contain endogenous buffers such as calmodulin, which, in their resting state diffuse almost as well as the EGTA–BAPTA molecules (Pusch and Neher, 1988). Some Ca-binding proteins appear to aid in diffusion of Ca. Kretsinger et al. (1982) modeled the contribution of intestinal calcium binding protein to aiding Ca movement from its entry on the lumenal side of intestinal cells to its exit point on the serosal side, as would be predicted for a diffusible exogenous buffer. This would apply to Ca-binding proteins, which do not themselves have receptors. However, many small Ca sensors such as calmodulin or troponin C act by binding to larger proteins, some of which are fixed. These physiological Ca buffers constitute an interesting hybrid, behaving as diffusible buffers in their Ca free state, but becoming less mobile, or fixed, in their Ca bound form. Clearly, our understanding of Ca distribution and receptors is in a rudimentary state.

Received for publication 1 July 1992 and in final form 9 September 1992.

REFERENCES

Adler, E. M., G. J. Augustine, S. N. Duffy, and M. P. Charlton. 1991. Alien intracellular calcium chelators attenuate neurotransmitter release at the squid giant synapse. *J. Neurosci.* 11:1496–1507.

Ahmed, Z., and J. A. Connor. 1988. Calcium regulation by and buffer capacity of molluscan neurons during calcium transients. *Cell Calcium.* 9:57–69.

Augustine, G. J., M. P. Charlton, and S. J. Smith. 1987. Calcium action in synaptic transmitter release. *Annu. Rev. Neurosci.* 10:633–693.

Augustine, G. J., and E. Neher. 1992. Calcium requirements for secretion in bovine chromaffin cells. *J. Physiol.* 450:247–271.

Blaustein, M. P. 1977. Effects of internal and external cations and of ATP on sodium-calcium exchange in squid axons. *Biophys. J.* 20:79–111.

Carafoli, E. 1987. Intracellular calcium homeostasis. *Annu. Rev. Biochem.* 56:395–433.

Chad, J. E., and R. Eckert. 1984. Calcium domains associated with individual channels can account for anomalous voltage relations of Ca-dependent responses. *Biophys. J.* 45:933–999.

Connor, J. A., Z. Ahmed, and G. Ebert. 1981. Diffusion of Ca, Ba, H^+ and arsenazo III in neuronal cytoplasm. *Soc. Neurosci. Abstr.* 7:15.

Connor, J. A., and G. Nikolakopoulou. 1982. Calcium diffusion and buffering in nerve cytoplasm. *Lect. Math. Life Sci.* 15:79–101.

Crank, J. 1975. The Mathematics of Diffusion. 2nd ed. Clarendon Press, Oxford. 414 pp.

Fenwick, E. M., A. Marty, and E. Neher. 1982. Sodium and calcium channels of bovine chromaffin cells. *J. Physiol.* 331:599–635.

Fogelson, A. L., and R. S. Zucker. 1985. Presynaptic calcium diffusion from various arrays of single channels. Implications for transmitter release and synaptic facilitation. *Biophys. J.* 48:1003–1017.

Grynkiewicz, G., M. Poenie, and R. Y. Tsien. 1985. A new generation of Ca^{2+} indicators with greatly improved fluorescence properties. *J. Biol. Chem.* 260:3340–3450.

Hernandez-Cruz, A., F. Sala, and P. R. Adams. 1990. Subcellular calcium transients visualized by confocal microscopy in a voltage-clamped vertebrate neuron. *Science (Wash. DC).* 247:858–862.

Hodgkin, A. L., and R. D. Keynes. 1957. Movements of labelled calcium in squid giant axons. *J. Physiol.* 138:253–281.

Irving, M., J. Maylie, N. L. Sizto, and W. K. Chandler. 1990. Intracellular diffusion in the presence of mobile buffers. Application to proton movement in muscle. *Biophys. J.* 57:717–721.

Kao, J. P. Y., and R. Y. Tsien. 1988. Ca2+ binding kinetics of fura-2 and azo-1 from temperature-jump relaxation measurements. *Biophys. J.* 53:635–639.

Konishi, M., A. Olson, S. Hollingworth, and S. M. Baylor. 1988. Myoplasmic binding of fura-2 investigated by steady-state fluorescence and absorbance measurements. *Biophys. J.* 54:1089–1104.

Kretsinger, R. H., J. E. Mann, and J. G. Simmonds. 1982. Model of facilitated diffusion of calcium by the intestinal calcium binding protein. *In* Vitamin D, Chemical, Biochemical and Clinical Endocrinology of Calcium Metabolism. Walter de Gruyter & Co., New York. 233–248.

Kushmerick, M. J., and R. J. Podolsky. 1969. Ionic mobility in muscle cells. *Science (Wash. DC).* 166:1297–1298.

Llinás, R., I. Z. Steinberg, and K. Walton. 1981. Relationship between presynaptic calcium current and postsynaptic potential in squid giant synapse. *Biophys. J.* 33:323–352.

Marty, A., and E. Neher. 1985. Potassium channels in cultured bovine adrenal chromaffin cells. *J. Physiol.* 367:117–141.

Neher, E. 1986. Concentration profiles of intracellular calcium in the presence of a diffusible chelator. *Exp. Brain Res. Ser.* 14:980–92.

Neher, E., and G. J. Augustine. 1992. Calcium gradients and buffers in bovine chromaffin cells. *J. Physiol.* 450:273–301.

Parnas, H., G. Hovav, and I. Parnas. 1989. Effect of Ca^{2+} diffusion on the time course of neurotransmitter release. *Biophys. J.* 55:859–874.

Pusch, M., and E. Neher. 1988. Rates of diffusional exchange between small cells and a measuring pipette. *Pfluegers Arch.* 411:204–211.

Rall, W. 1977. Core conductor theory and cable properties of neurons. *In* Handbook of Physiology. The nervous system. Am. Physiol. Soc., Bethesda, MD. 39–97.

Roberts, W. J., R. A. Jacobs, and A. J. Hudspeth. 1990. Colocalization of ion channels involved in frequency selectivity and synaptic transmission at presynaptic active zones of hair cells. *J. Neurosci.* 10:3664–3684.

Robinson, R. A., and R. H. Stokes. 1955. Electrolyte Solutions. Butterworths, London.

Sala, F. and Hernandez-Cruz, A. 1990. Calcium diffusion modeling in a spherical neuron. Relevance of buffering properties. *Biophys. J.* 57:313–324.

Seward, E. P., N. Chernevskaya, and M. C. Nowycky. 1992. Calcium entry, buffering and exocytosis in isolated peptidergic nerve terminals. *Neurosci. Soc. Abstr.* 18:246.

Simon, S. M., and R. R. Llinás. 1985. Compartmentalization of the submembrane calcium activity during calcium influx and its significance in transmitter release. *Biophys. J.* 48:485–498.

Smith, G. L., and D. J. Miller. 1985. Potentiometric measurements of stoichiometric and apparent affinity constants of EGTA for protons and divalent ions including calcium. *Biochim. Biophys. Acta.* 839:287–299.

Smith, P. D., G. W. Liesegang, R. L. Berger, G. Czerlinsk, and R. J. Podolsky. 1984. A stopped-flow investigation of calcium ion binding by EGTA. *Anal. Biochem.* 143:188–195.

Smith, S. J., and R. S. Zucker. 1980. Aequorin response facilitation and intracellular calcium accumulation in molluscan neurones. *J. Physiol.* 300:167–196.

Stockbridge, N., and J. W. Moore. 1984. Dynamics of intracellular calcium and its possible relationship to phasic transmitter release and facilitation at the frog neuromuscular junction. *J. Neurosci.* 4:803–811.

Strautman, A. F., R. J. Cork, and K. R. Robinson. 1990. The distribution of free calcium in transected spinal axons and its modulation by applied electrical fields. *J. Neurosci.* 10:3654–3575.

Thayer, S. A., and R. J. Miller. 1990. Regulation of intracellular free calcium concentration in single rat dorsal root ganglion neurones in vitro. *J. Physiol.* 425:85–115.

Thomas, P., A. Surprenant, and W. Almers. 1990. Cytosolic Ca^{2+}, exocytosis, and endocytosis in single melanotrophs of the rat pituitary. *Neuron.* 5:723–733.

Verhage, M., H. T. McMahon, W. E. J. M. Ghijsen, F. Boomsma, G. Scholten, W. Greet, V. M. Wiegant, and D. G. Nicholls. 1991. Differential release of amino acids, neuropeptides, and catecholamines from isolated nerve terminals. *Neuron.* 6:517–524.

Yamada, W. M., and R. S. Zucker. 1992. Time course of transmitter release calculated from simulations of a calcium diffusion model. *Biophys. J.* 61:671–782.